# Physics-guided deep image prior network for general zero-shot stain deconvolution

Jianan Chen[1,2,3] ✉, Lydia Y. Liu[1,4], Wenchao Han[2], Alison Cheung[2], Hubert Tsui[2], and Anne L. Martel[1,2] ✉

[1] Department of Medical Biophysics, University of Toronto, Toronto, ON, Canada
[2] Sunnybrook Research Institute, Toronto, ON, Canada
[3] UCL Cancer Institute, University College London, London, United Kingdom
[4] University Health Network, Toronto, ON, Canada
jianan.c@ucl.ac.uk; a.martel@utoronto.ca

**Abstract.** Many barriers remain before the clinical translation and deployment of prognostic and predictive models utilizing deep learning in digital pathology. In particular, models need to be generalizable to widespread variations in image characteristics resulting from differences in slide preparation protocols and inter-scanner variability. Yet, most existing stain deconvolution methods that correct for the variability in image appearances were developed and validated on specific datasets and perform poorly on unseen data. We developed Physics-Guided Deep Image Prior network for Stain deconvolution (PGDIPS), a self-supervised method guided by a novel optical physics model to perform zero-shot stain deconvolution and normalization. PGDIPS outperformed state-of-the-art approaches for the deconvolution of conventional stain combinations, enabled analysis of previously unsupported special stains, and provided superior interpretability by explicitly encoding representations for stain properties and the light transmittance/absorbance process. PGDIPS is publicly available as an end-to-end off-the-shelf tool at `https://github.com/GJiananChen/PGDIPS`.

**Keywords:** Digital Pathology · Stain Variation · Generalizability

## 1 Introduction

Computational pathology models extract quantitative features from digital pathology data, often in conjunction with clinical annotations and data from other omics domains, in order to aid disease diagnosis, treatment selection and drug target discovery [2, 16]. However, many hurdles remain to be overcome before advances in computational pathology can be translated into routine use [5]. In particular, the use of different slide preparation protocols and scanners across institutions requires models to be generalizable across images with widely varying characteristics [25]. This has led to an interest in stain deconvolution (SD) and stain normalization methods that aim to correct for variabilities in image appearances. Despite being a key pre-processing step in computational pathology, stain deconvolution remains an open problem [7].

Conventionally, SD is formulated as a matrix decomposition problem that deconvolutes the optical density of a stained slide into multiple paired color vectors and concentration maps [21]. Conventional SD methods are based on the Beer-Lambert Law, which relates, linearly, the attenuation of non-scattering light to the properties of the stained tissue through which the light is traveling [24]. Nevertheless, application of Beer's law is hindered under conditions of complex non-linear image formation ubiquitous in digital pathology images, for example due to saturation effects from high concentrations, scatter effects, or the presence of polychromatic light [19]. This leads to systemic deconvolution errors, especially for special stains [4, 9].

Deep-learning-based SD approaches have been proposed to alleviate the shortcomings of traditional SD methods [23]. As singly-stained slides are not routinely collected in clinical practice and rarely available for model training [7], most deep-learning-based SD models are designed to directly generate normalized images instead of explicitly performing stain deconvolution. Such processes depend on large, carefully curated datasets [8, 11, 12, 18, 22]. As a result of their data-driven nature, existing deep-learning-based SD methods exhibit impressive performance on the datasets they have been trained on, but struggle with generalizability on unseen data and unseen stains. As a complementary approach, stain augmentation has also been proposed as a more effective solution for addressing stain variations that could replace SD [25]. However, recent work has shown that even foundation models trained with extensive contrastive color augmentations are not robust to stain variations [10], suggesting that a re-evaluation of the value of classic SD methods may be in order.

As a result, conventional SD algorithms [17, 27, 30] remain the go-to methods for general SD tasks [1]. Yet, there continues to exist the need for an SD method that combines the strength of conventional and deep-learning-based SD algorithms, namely zero-shot, accrurate and generalizable. To address this gap, we propose Physics-Guided Deep Image Prior network for Stain deconvolution (PGDIPS), an end-to-end and zero-shot SD algorithm that can robustly and accurately deconvolute arbitrary numbers and types of stains. We extensively validated PGDIPS on different combinations of digital pathology stains and benchmarked PGDIPS against state-of-the-art zero-shot SD algorithms to demonstrate its superior applicability and performance.

## 2 Methods

PGDIPS implements an end-to-end neural network for the deconvolution of digital pathology images (**Figure 1**). PGDIPS represents a new paradigm for general stain deconvolution (SD) that features a self-supervised deep learning model whose training is guided by an optical physics model. More specifically, PGDIPS encodes an adapted Beer-Lambert model in its structure, and follows a deep image prior (DIP) training scheme to solve the model and perform stain deconvolution without the need for training data. PGDIPS can thus be readily applied to any type and number of stains.

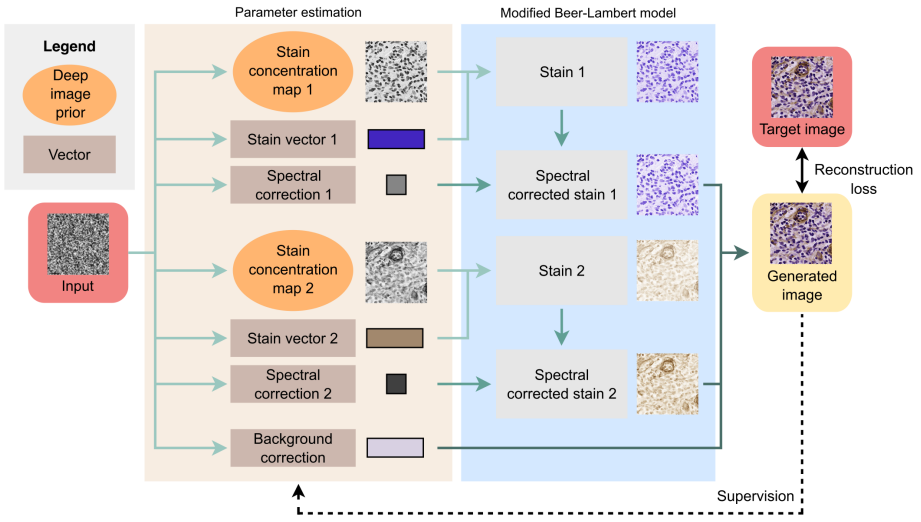


**Fig. 1.** PGDIPS network structure diagram featuring a modified Beer-Lambert model solved by components estimated by multiple deep image prior (DIP) modules.

**Deep Image Prior modules** A DIP network takes random noise as input and attempts to find a mapping that transforms the random noise into the target image [26]. During this zero-shot self-supervised process, the convolutional filters of the DIP network capture image-intrinsic priors as building blocks (*i.e.*, deep image priors) for reconstructing the target image. With the appropriate capacity, a DIP network will ignore high-frequency noise and learn the underlying image priors, making it a powerful method for image-inverse problems and image generation.

PGDIPS was inspired by Double-DIP [6], an algorithm that combined two DIPs using a simple linear equation to perform image decomposition tasks such as segmentation and dehazing. We extended this concept and assembled multiple DIP modules to estimate stain concentration maps $\boldsymbol{C}$ in our adapted optimal physics model, with the number of DIP modules corresponding to the number of stains to deconvolute. DIP modules follow the design of U-Net [20] and the structures described in [6].

**Problem formation** Following conventional SD methods [17,21], PGDIPS converts RGB intensities of the target image $\boldsymbol{I} \in \mathbb{R}^{w \times h \times 3}$ into corresponding optical density values $\boldsymbol{D} \in \mathbb{R}^{w \times h \times 3}$ by taking the logarithm of $\boldsymbol{I}$ normalized by the maximum possible Intensity $\boldsymbol{I}_0 = 255$. Based on the Beer-Lambert Law, the optical density values $\boldsymbol{D}$ can be decomposed into individual concentration maps $\boldsymbol{C} \in \mathbb{R}^{w \times h \times N}$ and stain color vectors $\boldsymbol{S} \in \mathbb{R}^{N \times 3}$ for $N$ types of stains (**Eq. 1**).

$$\boldsymbol{D} = -\log_{10}(\frac{\boldsymbol{I}}{\boldsymbol{I}_0}) = \boldsymbol{C}\boldsymbol{S} \tag{1}$$

**Spectral correction** To address systemic errors in SD caused by differences in the spectral properties of individual stains [9], we adapt the Beer-Lambert model by proposing a stain spectral correction factor $\boldsymbol{M} \in \mathbb{R}^N$ for each stain. For example, DAB is known to be a scatterer of light compared to hematoxylin [14], but in conventional SD models, DAB and hematoxylin are assumed to contribute equally to the final image. Adding a learnable weight $\boldsymbol{M}$ allows the deconvolution model to adjust the contribution of each stain accordingly.
**Background correction** In addition, background illumination may affect the perceived color of images captured by a scanner, and the effect may vary across different scanners. PGDIPS further estimates the effect of background illumination by capturing any consistent optical density that exists throughout the target image. This is achieved using a background illumination correction factor $\boldsymbol{B} \in \mathbb{R}^{1\times 3}$, which encodes the RGB channels of a uniform background illumination across the entire image patch.
**Objective & loss function** Given a target image, the main objective of PGDIPS is to train a model $\boldsymbol{F}(.)$ parameterized by a neural network $\theta$ that generates an image using the specified optical physics model that minimizes the pixel-wise difference between the generated image and the target image (**Eq. 2**):

$$\boldsymbol{F}_\theta(\boldsymbol{M}, \boldsymbol{C}, \boldsymbol{S}, \boldsymbol{B}) = \int |\boldsymbol{D} - \sum_{n=1}^{N} M_n \boldsymbol{C}_n \boldsymbol{S}_n - \mathbf{1}\boldsymbol{B}|^2 dx \tag{2}$$

where $\theta = \{\theta_1, \theta_2, ..., \theta_N\}$ denotes the weights of a series of DIP modules, $x$ denotes each pixel in the image $\boldsymbol{I}$ and $\mathbf{1} \in \mathbb{R}^{w\times h\times 1}$ is a matrix filled with ones. The loss function of PGDIPS consists of an MSE reconstruction loss derived from this main objective and an exclusion loss to encourage the separation of stains (**Eq. 3**):

$$L = \alpha L_{recon} + \beta L_{excl} \tag{3}$$

The exclusion loss reduces correlation between the gradient magnitudes of the predicted stain concentration maps (*e.g.*, hematoxylin *versus* eosin), calculated via element-wise multiplication of their normalized gradients across multiple spatial resolutions, as described in [29]. We empirically selected weights of loss functions, and applied the same set of loss weights $\alpha = 1$ and $\beta = 0.01$ for all experiments. Stain vectors, spectral correction factors and background correction factors are directly optimized.
**Stain normalization** As a direct downstream application of SD, stain normalization is typically performed by applying a standard set of stain color vectors from the target stain type to all estimated concentration maps [13, 27]. We augmented this approach by additionally applying the PGDIPS-estimated spectral correction factors and background illumination factor from the reference image, *i.e.* the image whose color style is used as the target for normalization.

## 3 Experiments

**Qualitative evaluation of zero-shot SD on various stains** Zero-shot stain deconvolution was performed using PGDIPS on six different types of staining

(**Fig. 2**), with comparisons to Macenko [17] and Vahadane [27] as they remain the most widely used zero-shot stain deconvolution (SD) techniques. While several recent deep-learning-based algorithms for stain normalization exist, they require large training datasets and are as a result both impractical and out-of-scope for the benchmarking of zero-shot SD methods [8, 11, 12, 18, 22].

**Quantitative evaluation metrics** Pearson correlation coefficient (PCC) and structural similarity index (SSIM) [28] were used for quantitative evaluation of SD results. PCC measures the linear correlation between stain concentration maps and ground truths, and SSIM quantifies the visual similarity and fidelity.

**Quantitative evaluation on H&E images** The performance of PGDIPS for H&E staining deconvolution was quantitatively evaluated against Macenko and Vahadane on a breast cancer dataset with paired H&E and immunofluorescence (mIF) DAPI images [3] (**Fig. 3a**). Co-registered DAPI images were used as the surrogate ground truth for hematoxylin deconvolution, as DAPI and hematoxylin both stain cell nucleus. Non-overlapping 512x512 H&E tiles were cropped from 81 images and filtered based on proportion of non-tissue background, resulting in 2008 tiles. DAPI mIF images were co-registered with the fixed H&E images using scale-invariant feature transform [15] followed by affine transformation.

**Quantitative evaluation on immunohistochemistry (IHC) images** The performance of PGDIPS for special stain deconvolution was benchmarked using the test set of DeepLIIF [7], which contains 598 sets of co-registered images with IHC hematoxylin and DAB staining, hematoxylin-only staining, mIF DAPI and mIF Ki-67 (**Fig. 3c**). Both hematoxylin-only staining and DAPI were used as the ground truth for hematoxylin deconvolution. Ki-67 was similary used as the label for DAB deconvolution, as Ki-67 and DAB both stain Ki-67-positive cells.

**Stain normalization and interpretability** Stain normalization was performed on the training set of MIDOG2022 [1], which contains 354 high-power field images of 150 human breast cancers and 204 canine tumors generated across 5 different types of scanners. Nine connected non-background 512x512 patches were randomly selected from each high-power field image to generate 3186 patches for the experiment. The vector parameters estimated by PGDIPS (*i.e.*, $\boldsymbol{M}, \boldsymbol{S}$, and $\boldsymbol{B}$) were visualized using t-SNE.

**Table 1.** PCC and SSIM of deconvoluted hematoxylin and co-registered DAPI for the breast H&E dataset. Values are denoted in mean ± std, n=2008.

| Method | PCC | p-value | SSIM | p-value |
|---|---|---|---|---|
| **Macenko** | 0.55 ± 0.17 | <0.01* | 0.35 ± 0.15 | <0.01* |
| **Vahadane** | 0.47 ± 0.13 | <0.01* | 0.24 ± 0.13 | <0.01* |
| **PGDIPS(ours)** | **0.59 ± 0.12** | Ref | **0.52 ± 0.12** | Ref |

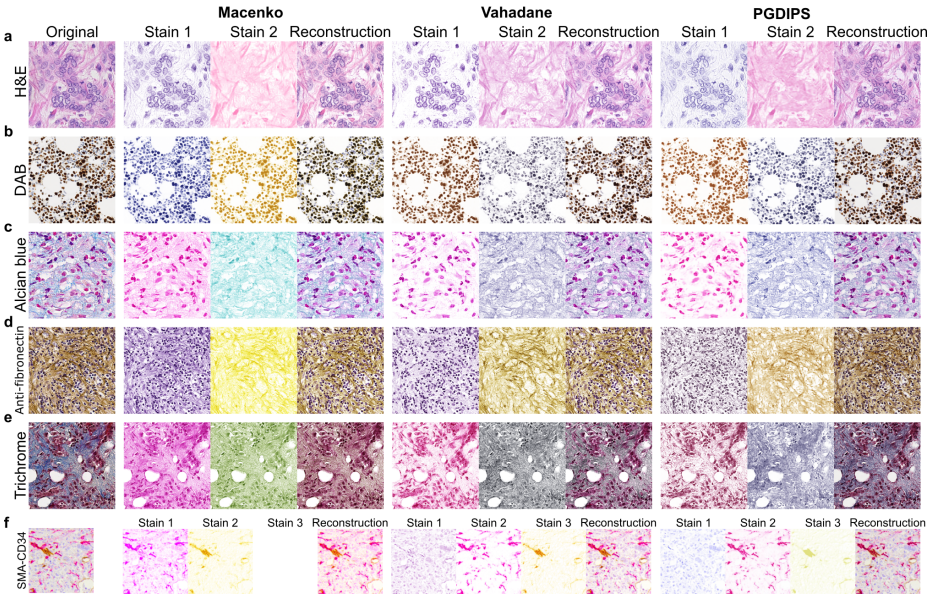


**Fig. 2.** Deconvolution of 6 different types of stains, with qualitative comparisons.

**Table 2.** PCC and SSIM of deconvoluted hematoxylin and co-registered hematoxylin-only staining (H) and DAPI (D), and deconvoluted DAB and co-registered Ki-67 (K) in the DeepLIIF IHC dataset. Values are denoted in mean ± std, n=598.

| Method | PCC (H) | p | SSIM (H) | p | PCC (D) | p | SSIM (D) | p |
|---|---|---|---|---|---|---|---|---|
| **Macenko** | 0.77±0.10 | * | 0.30±0.08 | * | 0.75±0.11 | * | 0.39±0.07 | * |
| **Vahadane** | 0.71±0.13 | * | 0.24±0.07 | * | 0.69±0.11 | * | 0.31±0.06 | * |
| **PGDIPS(ours)** | **0.81±0.10** | Ref | **0.46±0.11** | Ref | **0.79±0.11** | Ref | **0.59±0.12** | Ref |

| | PCC (K) | p | SSIM (K) | p |
|---|---|---|---|---|
| **Macenko** | 0.67±0.13 | * | 0.40±0.04 | * |
| **Vahadane** | 0.67±0.14 | * | 0.33±0.03 | * |
| **PGDIPS** | **0.72±0.13** | Ref | **0.77±0.10** | Ref |

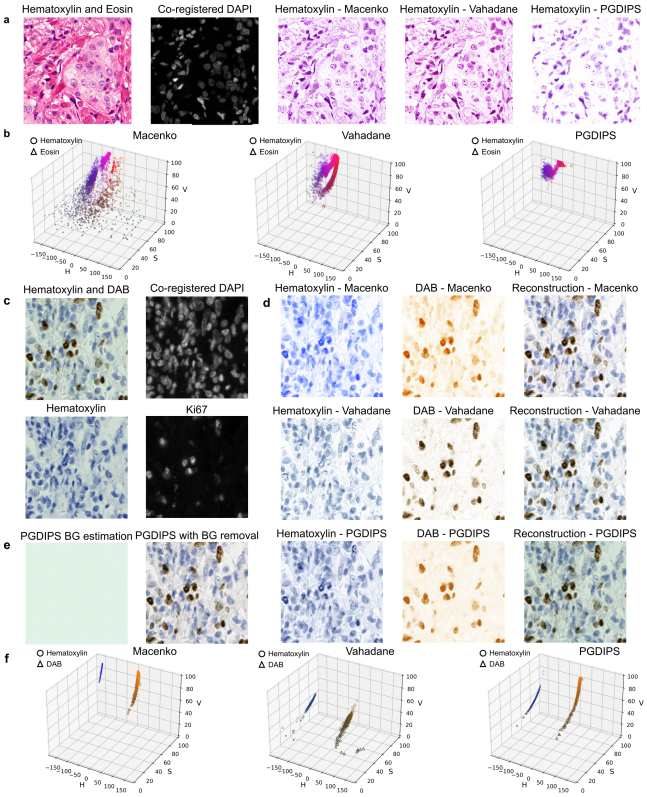


**Fig. 3.** **a**) Example H&E and DAPI image, and deconvolution results. **b**) Stain color vectors estimated in HSV color space, n = 2008. **c**) Example Hematoxylin&DAB, DAPI, Ki-67, and hematoxylin-only image. **d**) Deconvolution results. **e**) Estimated background illumination, **f**) Stain color vectors estimated in HSV color space, n = 598.

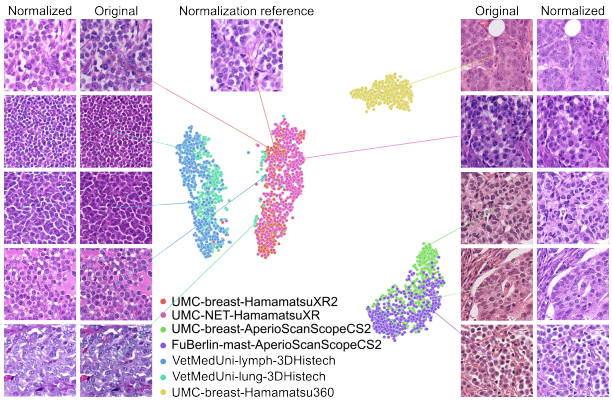


**Fig. 4.** PGDIPS-estimated parameters cluster by scanner type. Example stain-normalized images are shown alongside the original images.

## 4 Results

**Qualitative evaluation of zero-shot SD on various stains** PGDIPS achieved visually correct deconvolution across the stains tested without hyperparameter tuning (**Fig. 2a-f**). While Macenko and Vahadane especially had difficulties with the stain vectors of one or more special stains, PGDIPS produced reconstructed images with higher visual fidelity and colour vectors with higher visual accuracy. PGDIPS handled images of all dimensions and magnifications, and took 2GB of VRAM and 40 seconds to deconvolute an image tile of size 512x512, or on average 2 seconds per tile when inferencing on batches on a Nvidia A100 GPU.

**Quantitative evaluation on H&E images** PGDIPS achieved significantly higher deconvolution accuracy compared to Macenko and Vahadane, as measured by Pearson correlation coefficient (PCC) between the deconvoluted hematoxylin stain and the co-registered mIF DAPI image (**Table 1**). PGDIPS also performed substantially better in the structural similarity index (SSIM), a measure for tissue structure preservation [28], suggesting that its DIP-based design enabled better nuclei structure preservation, which may have implications for downstream analyses. The compact distribution of color vectors estimated by PGDIPS also reflected the performance stability of PGDIPS in a cohort of images processed with the same staining protocol and the same scanner (**Fig. 3b**).

**Quantitative evaluation on IHC images** The reconstructed images generated by PGDIPS harboured greater visual resemblance to the target images, compared to Macenko and Vahadane (**Fig. 3d**), in part due to its ability to estimate and isolate the background illumination (**Fig. 3e**). PGDIPS also achieved significantly superior performance in deconvolution accuracy and structure preservation for hematoxylin deconvolution, both when using mIF DAPI and hematoxylin-only staining as the ground truth (**Table 2**). PGDIPS performed similarly well in deconvolution accuracy and cell structure preservation for DAB deconvolution, evaluated against mIF Ki67. In contrast, color vectors estimated by Macenko were consistently biased and led to spurious concentrations in the deconvoluted DAB layer, while cell structures were poorly preserved by Vahadane in the deconvoluted hematoxylin layer. Greater variation in color vectors was observed in the DeepLIIF test set, likely caused by differential presence of Ki67-positive cells (**Fig. 3f**). These findings underscore the challenges of special stain deconvolution and validate the generalizability of PGDIPS.

**Stain normalization and interpretability** Stain normalization using PGDIPS achieved visually consistent appearance in the MIDOG 2022 dataset, across different studies, scanners, and tissue types, corroborating the accuracy of parameter inference by PGDIPS. Visualization of PGDIPS-estimated paramters after dimensionality reduction revealed the clustering of images driven by scanner type, despite differences in tissue types and centers, highlighting the importance of correcting for inter-scanner variability prior to downstream tasks (**Fig. 4**).

## 5 Conclusions and Discussion

We present PGDIPS, an algorithm for zero-shot general stain deconvolution. PGDIPS focuses on strong generalizability without the need for expert knowledge, data collection or hyperparameter tuning, and outperformed existing zero-shot SD approaches in a variety of stain types. We have made PGDIPS an easily accessible off-the-shelf tool for general-purpose SD that could be incorporated into most digital pathology workflows.

Currently, deep-learning-based algorithms operate on image tiles and require stitching to generate whole slide image (WSI)-level results. This could lead to checkerboard artifacts due to intra-slide stain variabilities. In future studies, we will analyze WSI processing stability and investigate ways to generate robust yet variability-aware WSI-level SD results. We will also, in subsequent work, compare PGDIPS with non-zero-shot deep generative methods. PGDIPS represents a new paradigm in physics-guided stain deconvolution and normalization, one we believe will inspire novel research and methodology development.

**Acknowledgments.** The authors would like to thank the Natural Sciences and Engineering Research Council of Canada (NSERC) for funding. Jianan Chen is supported by the Marie Curie Postdoctoral Fellowship (101210483).

**Disclosure of Interests.** The authors have no competing interests to declare that are relevant to the content of this article.

## References

1. Aubreville, M., Stathonikos, N., Bertram, C.A., Klopfleisch, R., Ter Hoeve, N., Ciompi, F., Wilm, F., Marzahl, C., Donovan, T.A., Maier, A., et al.: Mitosis domain generalization in histopathology images—the midog challenge. Medical Image Analysis **84**, 102699 (2023)
2. Campanella, G., Hanna, M.G., Geneslaw, L., Miraflor, A., Werneck Krauss Silva, V., Busam, K.J., Brogi, E., Reuter, V.E., Klimstra, D.S., Fuchs, T.J.: Clinical-grade computational pathology using weakly supervised deep learning on whole slide images. Nature medicine **25**(8), 1301–1309 (2019)
3. Cheung, A.M.Y., Wang, D., Liu, K., Hope, T., Murray, M., Ginty, F., Nofech-Mozes, S., Martel, A.L., Yaffe, M.J.: Quantitative single-cell analysis of immunofluorescence protein multiplex images illustrates biomarker spatial heterogeneity within breast cancer subtypes. Breast Cancer Research **23**, 1–17 (2021)
4. Clarke, E.L., Treanor, D.: Colour in digital pathology: a review. Histopathology **70**(2), 153–163 (2017)
5. Cui, M., Zhang, D.Y.: Artificial intelligence and computational pathology. Laboratory Investigation **101**(4), 412–422 (2021)
6. Gandelsman, Y., Shocher, A., Irani, M.: " double-dip": unsupervised image decomposition via coupled deep-image-priors. In: Proceedings of the IEEE/CVF conference on computer vision and pattern recognition. pp. 11026–11035 (2019)
7. Ghahremani, P., Li, Y., Kaufman, A., Vanguri, R., Greenwald, N., Angelo, M., Hollmann, T.J., Nadeem, S.: Deep learning-inferred multiplex immunofluorescence for immunohistochemical image quantification. Nature machine intelligence **4**(4), 401–412 (2022)

8. Gupta, A., Duggal, R., Gehlot, S., Gupta, R., Mangal, A., Kumar, L., Thakkar, N., Satpathy, D.: Gcti-sn: Geometry-inspired chemical and tissue invariant stain normalization of microscopic medical images. Medical Image Analysis **65**, 101788 (2020)
9. Haub, P., Meckel, T.: A model based survey of colour deconvolution in diagnostic brightfield microscopy: Error estimation and spectral consideration. Scientific reports **5**(1), 12096 (2015)
10. de Jong, E.D., Marcus, E., Teuwen, J.: Current pathology foundation models are unrobust to medical center differences. arXiv preprint arXiv:2501.18055 (2025)
11. Kang, H., Luo, D., Feng, W., Zeng, S., Quan, T., Hu, J., Liu, X.: Stainnet: a fast and robust stain normalization network. Frontiers in Medicine **8**, 746307 (2021)
12. Ke, J., Shen, Y., Liang, X., Shen, D.: Contrastive learning based stain normalization across multiple tumor in histopathology. In: International Conference on Medical Image Computing and Computer-Assisted Intervention. pp. 571–580. Springer (2021)
13. Khan, A.M., Rajpoot, N., Treanor, D., Magee, D.: A nonlinear mapping approach to stain normalization in digital histopathology images using image-specific color deconvolution. IEEE transactions on Biomedical Engineering **61**(6), 1729–1738 (2014)
14. Leong, F.W., Brady, M., McGee, J.O.: Correction of uneven illumination (vignetting) in digital microscopy images. Journal of clinical pathology **56**(8), 619–621 (2003)
15. Lowe, D.G.: Distinctive image features from scale-invariant keypoints. International journal of computer vision **60**, 91–110 (2004)
16. Lu, M.Y., Chen, T.Y., Williamson, D.F., Zhao, M., Shady, M., Lipkova, J., Mahmood, F.: Ai-based pathology predicts origins for cancers of unknown primary. Nature **594**(7861), 106–110 (2021)
17. Macenko, M., Niethammer, M., Marron, J.S., Borland, D., Woosley, J.T., Guan, X., Schmitt, C., Thomas, N.E.: A method for normalizing histology slides for quantitative analysis. In: 2009 IEEE international symposium on biomedical imaging: from nano to macro. pp. 1107–1110. IEEE (2009)
18. Mahapatra, D., Bozorgtabar, B., Thiran, J.P., Shao, L.: Structure preserving stain normalization of histopathology images using self supervised semantic guidance. In: Medical Image Computing and Computer Assisted Intervention–MICCAI 2020: 23rd International Conference, Lima, Peru, October 4–8, 2020, Proceedings, Part V 23. pp. 309–319. Springer (2020)
19. Oshina, I., Spigulis, J.: Beer–lambert law for optical tissue diagnostics: current state of the art and the main limitations. Journal of biomedical optics **26**(10), 100901–100901 (2021)
20. Ronneberger, O., Fischer, P., Brox, T.: U-net: Convolutional networks for biomedical image segmentation. In: Medical image computing and computer-assisted intervention–MICCAI 2015: 18th international conference, Munich, Germany, October 5-9, 2015, proceedings, part III 18. pp. 234–241. Springer (2015)
21. Ruifrok, A.C., Johnston, D.A.: Quantification of histochemical staining by color deconvolution. Analytical and Quantitative Cytology and Histology **23**(4), 291–299 (2001)
22. Shaban, M.T., Baur, C., Navab, N., Albarqouni, S.: Staingan: Stain style transfer for digital histological images. In: 2019 Ieee 16th international symposium on biomedical imaging (Isbi 2019). pp. 953–956. IEEE (2019)
23. Srinidhi, C.L., Ciga, O., Martel, A.L.: Deep neural network models for computational histopathology: A survey. Medical image analysis **67**, 101813 (2021)

24. Swinehart, D.F.: The Beer-Lambert Law. Journal of Chemical Education **39**(7), 333 (1962)
25. Tellez, D., Litjens, G., Bándi, P., Bulten, W., Bokhorst, J.M., Ciompi, F., Van Der Laak, J.: Quantifying the effects of data augmentation and stain color normalization in convolutional neural networks for computational pathology. Medical image analysis **58**, 101544 (2019)
26. Ulyanov, D., Vedaldi, A., Lempitsky, V.: Deep image prior. In: Proceedings of the IEEE conference on computer vision and pattern recognition. pp. 9446–9454 (2018)
27. Vahadane, A., Peng, T., Sethi, A., Albarqouni, S., Wang, L., Baust, M., Steiger, K., Schlitter, A.M., Esposito, I., Navab, N.: Structure-preserving color normalization and sparse stain separation for histological images. IEEE transactions on medical imaging **35**(8), 1962–1971 (2016)
28. Wang, Z., Bovik, A.C., Sheikh, H.R., Simoncelli, E.P.: Image quality assessment: from error visibility to structural similarity. IEEE transactions on image processing **13**(4), 600–612 (2004)
29. Zhang, X., Ng, R., Chen, Q.: Single image reflection separation with perceptual losses. In: Proceedings of the IEEE conference on computer vision and pattern recognition. pp. 4786–4794 (2018)
30. Zheng, Y., Jiang, Z., Zhang, H., Xie, F., Shi, J., Xue, C.: Adaptive color deconvolution for histological wsi normalization. Computer methods and programs in biomedicine **170**, 107–120 (2019)